Full dense CoSb3 single phase with high thermoelectric performance prepared by oscillated cooling method

Full Dense $CoSb_3$ single phase with high thermoelectric performance prepared by Oscillated Cooling Method

Babak Alinejad, Alberto Castellero, Marcello Baricco

Laboratory of Metallurgy, Department of Chemistry, University of Turin, Via P.Giuria, 9, I-10125, Torino, Italy

*Corresponding author. Tel.: +39 3804752983; E-mail address: babak.alinejad@edu.unito.it; alinejad_bk@yahoo.com

A new mechanism is established for preventing porosity formation in the microstructure of $CoSb_3$ phase during peritectic solidification. Phase and microstructure analysis at different stages of solidification revealed that oscillated cooling could hinder spontaneous nucleation, improve homogenous nucleation, limit the number of primary grains and impose planar growth. These factors enhance melt flux during peritectic solidification and prevent porosity formation due to phase transformation contraction. By utilizing this method, dense single phase of $CoSb_3$ could be obtained in single batch process without any post treatment. Highest power factor of 55$\mu Wcm^{-1}K^{-2}$ was measured at 550°C.

Keywords: peritectic solidification, thermoelectric materials, crystallization, microstructure, full dense.

Thermoelectric materials equip us to encounter upcoming energy crisis by recycling the heat wasted in power plants and engine exhausts, posing no threat to already endangered earth environment [1,2]. For medium-temperature thermoelectric applications, CoSb-based skutterudites have been extensively studied [3], among them; $CoSb_3$ is the most qualified skutterudite compound [4]. According to the literatures, adding Yb into structure of $CoSb_3$ enhances its thermoelectric properties by decreasing thermal conductivity and enhancing n-type conductivity [5]. Phase transformations in Co-Sb system is distinguished by 3 different stages in Sb-rich region and $CoSb_3$ phase is theoretically obtained from melts after two peritectic transformations (Fig.1A) [6]. Practically, because of sluggish peritectic transformation, annealing treatment is needed to gain $CoSb_3$ single-phase [7]. Due to low concentration of Yb in partially filled skutterudite (Yb<10 at %), Co-Sb binary-phase diagram is used for simplification [6]. Peritectic solidification involves nucleation and growth of primary phase followed by reaction of primary phase with remnant liquid phase to obtain second phase. The second step is mainly controlled by atomic diffusion and, therefore, usually a combination of primary and secondary phases is obtained after solidification [8,9]. However, one can obtain single-phase by subsequent annealing [4]. During solidification, dendritic growth of primary phase entraps liquid phase in the dendritic arms. This prevents liquid from filling the spaces left by peritectic phase transition, producing porosity [6,8,9]. Solidification contraction rate for phase transitions (2) and (3) are 7% and 0.1%, respectively (Fig.1A); implying that reaction (2) is responsible for solidification contraction during peritectic phase transition [6]. Nevertheless, real value of porosity is usually much more than 10% because as dendrites grow, a capillary network of interdendritic melt is formed among the dendrites [10], decreasing the temperature, dendrites grow even more, and remained melt is entrapped in dendrites arms and capillary network connection is lost. Hence, melt fails to fill free spaces emerged

from density difference between $CoSb_2$ and L(Sb)+CoSb phases in the first peritectic transitions [6]. Resultant porosity percentage strongly depends on dendrites length, space among them and growth rates of dendrites and their branches. This porosity is superimposed with ~3% shrinkage due to isolated melt contraction during the last step of solidification, which depends on transformation fraction. Producing dense $CoSb_3$ single phase sounds very appealing because both impurity and porosity diminish thermoelectric properties. Porosities make joining process more intricate and incompetent for fabrication of thermoelectric devices. A common (but not fully successful) procedure for preparing $CoSb_3$ from melt is Bridgman method that results in multiphase and inhomogeneous ingot, again causing porosity after annealing trial for gaining single-phase [11,12]. Although growth of the $CoSb_3$ single crystal has been reported in ref.[13], but achievement of fully dense $CoSb_3$ single-phase was not validated by structure and microstructure investigations. In the mentioned work, only tip of the crystal has been reported to be dense while the rest is Sb-rich eutectic which is normally porous due to evaporation of excess Sb when thermoelectric is exposed to working temperature. So far, gaining fully dense $CoSb_3$ from melt has been a challenge for researchers. Even 95% of theoretical density has been considered as a significant success which is obtained by controlling the melting temperature and employing proper starting materials. However, still some impurities (Sb and $CoSb_2$) remain [6]. Other methods (e.g. rapid solidification) need complementary techniques like SPS [14] to obtain highly dense $CoSb_3$ [15] but temperature gradient of sintering process causes heterogeneity in sample density [16]. Therefore, SPS cannot be considered as appropriate procedures to produce industrial and commercial thermoelectric products. Hence, producing fully dense $CoSb_3$ using a single process step still remains the Holy Grail.

This work introduces a method for porosity elimination in $CoSb_3$ microstructure using oscillated cooling (OC) method. We also suggest a new mechanism for solidification in this innovative technique [17]. Effects of OC on nucleation, grain growth and porosity prevention in $CoSb_3$ microstructure are described in detail. Two control samples were utilized for comparison: one was cooled in air after being removed from furnace followed by subsequent annealing, while the other is cooled monotonically in furnace with a pure cooling rate equal to average rate of OC. Interpretation of result helps us understand more about solidification and microstructure of $CoSb_3$ produced by OC.

Elemental cobalt powder (purity 99.95%), antimony shot (purity 99.999%) and Ytterbium (99.999%) were weighted ~16g according to stoichiometry $Yb_{0.25}Co_4Sb_{12}$. Five samples were prepared for different procedures (Fig.1B). The mixed powder was poured into quartz ampoule with diameter of 1cm, sealed under vacuum of 5×10^{-5}torr and placed into a muffle furnace. Length of the ampoule was 7cm after sealing. The muffle slowly warmed up from room temperature to 1200°C with rate of 5°C/min and maintained at this temperature for 2h.

Then five samples were prepared:

A: brought out from furnace and cooled down in air. The resulted sample was then annealed at 600°C for 48h.

B: underwent a monotonic slow cooling in furnace with rate of 20°C/h.

C: “OC procedure (5°C/step)” which implies periodic 5°C temperature increment followed by 10°C decrease with average cooling rate of 20°C/h, down to 800°C (to preserve solidification front for subsequent metallographic examination).

D: same as sample C, except that oscillation stopped at 700°C.

E: same as sample C, except that oscillation stopped at 600°C.

Some isothermal heat-treatments were applied on samples B, C, D and E to reach equilibrium condition as shown in Fig. 1B.

Microstructures of the samples were studied by both optical and Scanning Electron Microscopy (SEM, Leica Stereoscan 410 instrument) equipped with an energy dispersion spectroscopy (EDS) microprobe (Oxford Instruments) operating at 25kV and X-ray diffraction analysis using PW3040/60 X'Pert PRO MPD diffractometer operating at 40kV and 30mA with CuKα radiation (λ=1.5405Å). Composition of samples was investigated by EDS installed on SEM instrument to confirm different phases. Densities of samples A, B and E were measured by Archimedean method. Seebeck coefficient and electrical conductivity were measured by standard temperature differential and 4-point-probe methods from 25°C to 600°C.

Sample B was single-phase just after solidification, but contained numerous pores of size 100-300µm and very fine voids of size 1-3µm (Fig.2.B), resulting in 89% of theoretical density. Fig.2.C represents the second peritectic phase transformation in sample C, self-assembled grains with regular geometry containing $CoSb_2$ cores and $CoSb_3$ shells in faceted polygonal shapes encompassed by residual Sb. Average size of primary grains in sample C is 200µm with a density of ~10/mm^2. Fig.2.D illustrates that peritectic transformation in sample D has progressed more compared with sample C. Residual Sb and $CoSb_2$ phase in sample D are less than those in sample C and $CoSb_3$ is dominant phase (Fig.2.D and S.Fig.2). Sample E was single-phase having 99.6% of theoretical density as confirmed by Archimedean method. EDX results were confirmed by XRD results (S.Fig.2 and Fig.4). Hence, continuing OC to 600°C, peritectic transformation is accomplished (Fig. 2.E).

According to binary-phase diagram of Co-Sb system, by reducing temperature from ~1000°C, atoms are rather arranged and embryos are formed in the melt and transformed to CoSb nuclei. Increasing temperature during oscillation eliminates most of unstable nuclei and by the next temperature decrease, nucleation starts again. Repeating this process, few nucleuses (only larger ones) survive [18] which results in limited number of primary grains (Fig.2.C). Fig.3.A shows faceted primary grains having multi ledges with no evidence of dendritic structure. Clear faceted grains show that the grains are well-crystallized. Ledge shapes indicate that lateral growth is dominant mechanism. Therefore, dendritic shape cannot be stable and faceted grains are formed by remelting of dendrite tips at the peak of each temperature oscillation cycle. This phenomenon can also be explained by effect of OC on reversing heat transfer direction. In typical solidification, center of melt is hotter than outer part and, knowing the fact that primary dendrites grow in direction of heat transfer, [19] temperature increase during slow cooling reverses heat transfer direction and helps dendrites tip to melt and prepares condition of lateral growth. In fact, using temperature oscillation, heat transfer from melt center to mold surface (quarts tube) is reversed periodically. This swaying heat transfer pattern is experienced by all materials in quarts tube (melts and primary grains). Since growth direction of primary dendrites depends on heat transfer from dendrite tip to the facing melt, [19] tendency for dendrite growth is periodically controlled by branches tip melting. Since heat transfer from furnace chamber to the sample center is isotropic, grains growth is identical in all three dimensions and there is no elongation in the grains. It seems that the

ampoule size was sufficiently small and duration of each cycle was long enough for whole sample to sense temperature oscillation homogenously. Decreasing temperature to less than 930°C, the first peritectic phase transformation starts. Diffusion of Sb atoms into CoSb grains forms $CoSb_2$ phase. Continuing cooling process to below 875°C, the second peritectic phase transfer starts. As it can be concluded from Fig.2.C.1 and Fig.3.A, whole CoSb phase is then consumed, so the first peritectic is completed in sample C. Comparing fig.2.C.2 and fig.3.A, it is found that grain boundaries increase dramatically while CoSb phase transforms to $CoSb_2$. Diffusion of Sb atoms into $CoSb_2$ grains forms a narrow shell of $CoSb_3$ phase around $CoSb_2$ cores (Fig.2.C.1). Subsequently, antimony diffuses from Sb-rich melt through $CoSb_3$ toward $CoSb_2$ grains and reacts with $CoSb_2$ to increase $CoSb_3$ phase. Fig.3.B illustrates sample C at higher magnification shows a grain (with a small rectangular tooth of $CoSb_3$ phase) which has stopped lateral growth in antimony phase; indicating that lateral growth is also dominant in second peritectic solidification. The cross-section of sample D including area of grown crystal near the wall of quartz ampoule is shown in Fig.3.D.2. In traditional solidification, mold vicinities are heterogeneous nucleation sites. However, as depicted in the sample cross-section, mold vicinities are not saturated with primary grains (grains are formed sparsely and distant from the mold). Distribution of the grains is uniform both near and far from the mold. This implies that, using OC method, heterogeneous nucleation is superseded by homogeneous nucleation. The OC-method ability to eliminate closed shrinkage can be concluded from fig.3.D.1 where even with diminutive liquid trapped in the last steps of solidification, the microstructure shows no closed shrinkage and ingot cross-section is completely porous-free. If the melt had no possibility for moving in 3D capillary network through open paths, there would be 3% porosity in areas containing Sb where the last solidification would happen. However, no porosity is found in fig.2.D.1, implying that although the solidification is more than 90% complete, number, arrangement and form of grains provide intergranular melt capillary network still open and functional for feeding solidification and compensating the shrinkage.

Continuing OC down to 600°C (sample E), second peritectic completes and single-phase is achieved with $CoSb_3$ grains nearly uniform and highly cohesive. The SEM image shows that grains are closely packed also Archimedean method confirmed a 99.6% of theoretical density. There are two distinguishable types of grains (Fig.2.E.2): fine elongated column-like grains (with average size of ~2μm, emerged from peritectic transformations of $CoSb_2$ to $CoSb_3$), and equiaxed grains (less than 5μm, emerged from Sb-rich region between primary grains in last solidification stage).

Complete pattern Rietveld refinement analysis of sample E by MAUD software [20,21] is depicted in Fig.4. Difference between calculated and experimental patterns is almost zero in entire 2θ ranges, indicating that good refinements were performed and calculated lattice parameter for sample E by Rietveld refinement (i.e., 9.046Å) is reliable. This value is slightly higher than 9.0347Å (standard lattice parameter of pure $CoSb_3$ phase [22]), indicating that Yb was successfully inserted in vacant sites of $CoSb_3$. Since diffusion efficiency of grain boundary can be hundred times higher than that of mass, and since enormous grain boundaries were formed (Fig.2.E.1), one can explain high purity of $CoSb_3$ achieved by this technique.

Seebeck coefficients of samples differ slightly but electrical conductivity of sample B is almost 60% of sample E; although, difference in densities is less than 10%. This shows adverse effect of porosity on electrical conductivity. Sample E has a high power factor of $55\mu Wcm^{-1}K^{-2}$, comparable to previous report for n-type $CoSb_3$ made by powder

metallurgical process [5]. It should be noted that $CoSb_3$ phase prepared in the current work has high homogeneity which could not be obtained by typical powder metallurgical process.

A new OC was developed to eliminate porosity in $CoSb_3$ peritectic alloy microstructure. Results showed that, with continuous OC down to 600°C, fully dense single-phase of $CoSb_3$ could be obtained and highest power factor of 55$\mu Wcm^{-1}K^{-2}$ was measured for obtained thermoelectric materials at 550°C while the sample with more than 10% porosity and power factor of 27 $\mu Wcm^{-1}K^{-2}$ (less than half of the sample prepared by OC method) obtained by typical monotonic slow cooling in furnace with the same average cooling rate.

References:

1. D. M. Rowe. CRC Handbook of Thermoelectrics, CRC press, New York, 2005.
2. R. Funahashi, M. Mikami, T. Mihare, S. Urata and N. Ando, J. Appl. Phys. 99 (2006) 066117-20.
3. C. Zhou, D. Morelli, X. Zhou, G. Wang and C. Uher, Intermetallics. 19 (2011) 1390-93.
4. Y. Kawaharada, K. Kurosaki, M. Uno and S. Yamanaka, J. Alloy. Compd. 315 (2001) 193-97.
5. T. Dahal, Q. Jie, G. Joshi, S. Chen, C. Guo and Y. Lan, Acta. Materialia. 75 (2014) 316-21.
6. H. Y. Geng, S. Ochi and J.Q. Guo, Appl. Phys. Lett. 91(2007) 022106-9.
7. I. H. Kim, J. I. Lee, S. C. Ur, K W. Jang and J. S.Kim, Solid. State. Phenomena. 118 (2006) 565-70.
8. K. Biswas, R. Hermann, H. Wendrock, J. Priede, G. Gerbeth and B. Buechner, J. Alloys. Compd. 480 (2009) 295-98.
9. W. Zhai and B. Wei, Mater. Lett. 108 (2013) 145-48.
10. L. Zheng, G. Zhang, C. Xiao, T. L. Lee, B. Han, Z. Lee, D. Daisenberger and J. Mi, Scripta. Materialia. 74 (2014) 84-87.
11. M. Akasaka, T. Iida, G. Sakuragi, S. Furuyama, M. Noda, S. Matsui, M. Ota, H. Suzuki, H. Satu, Y. Takanashi and S. Sakuragi, J. Alloys. Compounds. 386 (2005) 228-33.
12. S. Furuyama, T. Lida, S. Matsui, M. Akasaka, M. Nishio and Y. Takanashi, J. Alloy. Compounds. 415 (2006) 251-56.
13. T. Caillat, J. Fleurial, A. Borshchevsky, Crystal. Growth. 166 (1996) 722-26.
14. X. Su, H. Li, Y. Yan, G. Wang, H. Chi, X. Zhou, X. Tang, Q.Zhang and C. Uher, Acta. Materialia. 60 (2012) 3536-44.
15. J. Zhang, Q. Lu, K. Liu, L. Zhang and M. Zhou, Mater. Lett. 58 (2004) 1981-84.
16. M. Suárez, A. Fernández, J. L. Menéndez, R. Torrecillas, H. U. Kessel, J. Hennicke, R. Kirchner and T. Kessel, Challenges and Opportunities for Spark Plasma Sintering: A Key Technology for a New Generation of Materials, in: Burcu Ertuğ, Sintering Applications, Intech., Hampshire, 2013, pp. 321-22.
17. A. Castellero, B. Alinejad and M.Baricco, Proc. Intl. Conf. Thermoelectrics 34 (2015) 40-41.
18. W. Hintzmann and G. M. Vogt, J. Crystal. Growth. 5 (1969) 274-78.
19. D.A. Porter and K. E. Easterling. Phase transformations in metals and alloys, Chapman & Hall, London, 1992.
20. L. Lutterotti, S. Matthies, H. Wenk, A. Schultz and J. Richardson, J. Appl. Phys. 8 (1997) 1594-1600.
21. N. M. Torkaman, Y. Ganjkhanlou, M. Kazemzad and H. H. Dabaghi, Material. Characterization. 61 (2010) 362-70.
22. N. R. Dilley, E. D. Bauer, M. B. Maple, B. C. Sales, J. Appl. Phys. 88 (2000) 1948-51.

Figure Captions:

Fig.1. A) phase diagram of Co-Sb system. B) Time-Temperature Curve for solidification of different samples (Sample B using monotonic slow cooling and samples C, D and E using Oscillated cooling method).

Fig.2. Effect of different cooling program on microstructure of the samples was investigated by BS.SEM. B: Microstructure of sample B which is prepared using monotonic slow cooling. C, D and E illustrate Different step progression in peritectic solidification in sample C, D and E respectively. (Insets illustrate samples with higher magnification).

Fig.3 A) Faceted primary grains having multi ledges indicate lateral growth before completing first peritectic transformation and B) rectangular tooth indicated lateral growth during second peritectic solidification.

Fig.4. Rietvled refinement performed on Sample E (experimental, calculated and differences of them are shown)

Fig. 1

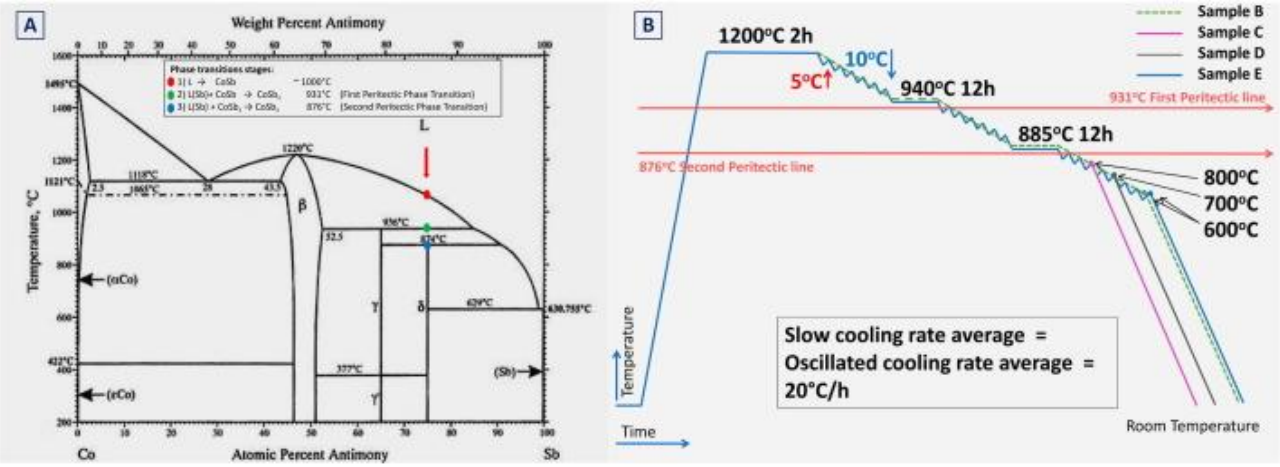
A
Weight Percent Antimony
Phase transitions stages:
1) L → CoSb ~ 1000°C
2) L(Sb)+ CoSb → CoSb2 931°C (First Peritectic Phase Transition)
3) L(Sb) + CoSb2 → CoSb3 876°C (Second Peritectic Phase Transition)
Temperature, °C
Atomic Percent Antimony
Co
Sb
L
β
γ
δ
γ'
(αCo)
(εCo)
(Sb)
B
1200°C 2h
10°C
5°C
940°C 12h
931°C First Peritectic line
885°C 12h
876°C Second Peritectic line
800°C
700°C
600°C
Sample B
Sample C
Sample D
Sample E
Slow cooling rate average =
Oscillated cooling rate average =
20°C/h
Temperature
Time
Room Temperature

Fig. 2

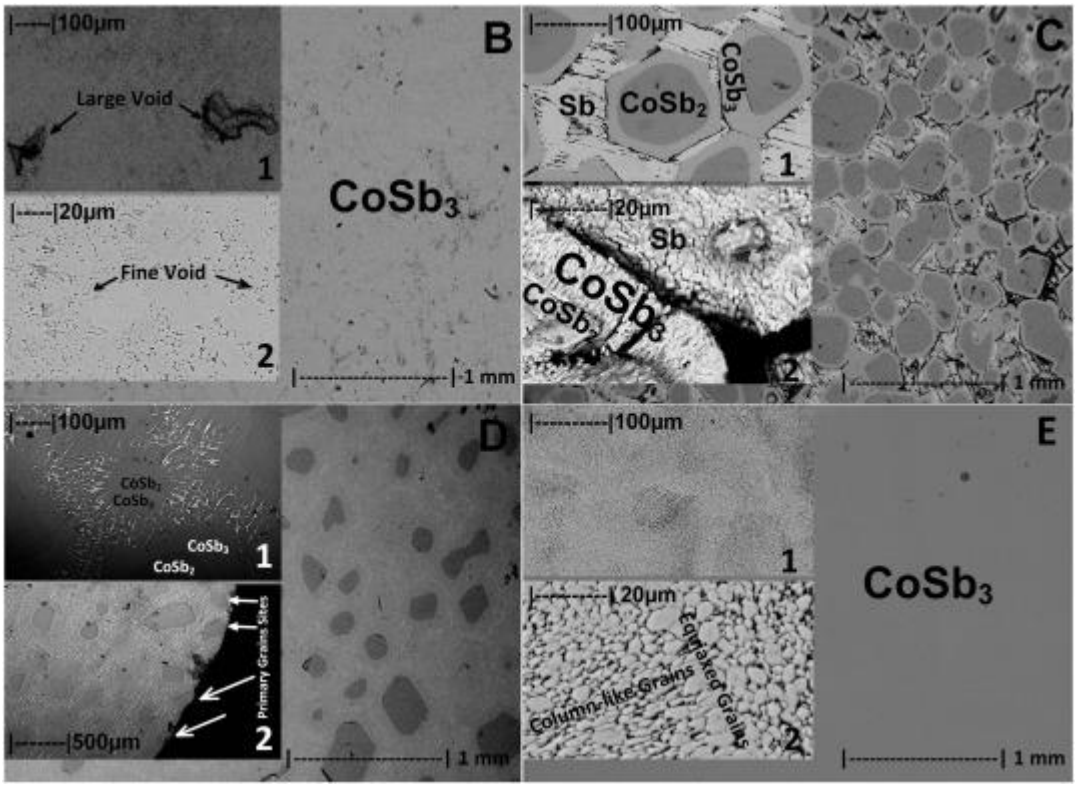
100μm
Large Void
1
B
CoSb3
20μm
Fine Void
2
1 mm
100μm
Sb
CoSb2
CoSb3
1
C
20μm
Sb
CoSb3
CoSb2
2
1 mm
100μm
CoSb2
CoSb3
CoSb3
CoSb2
1
D
500μm
Primary Grains Sites
2
1 mm
100μm
1
E
CoSb3
20μm
Equiaxed Grains
Column-like Grains
2
1 mm

Fig. 3

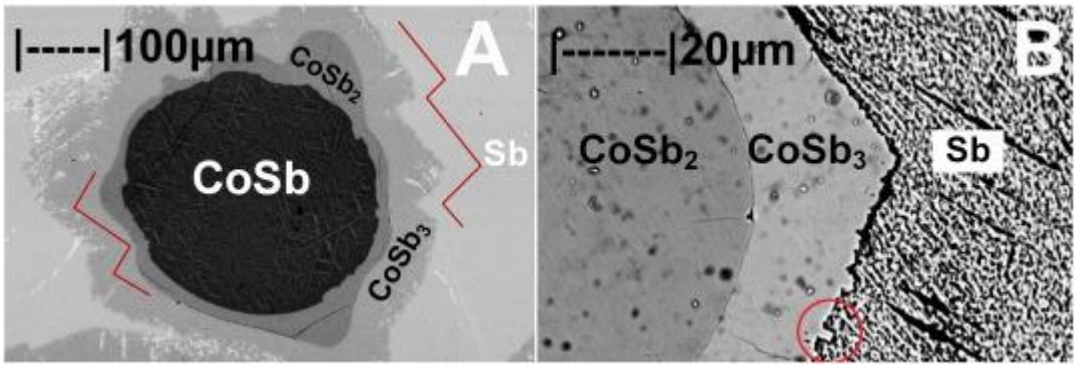

Fig. 4

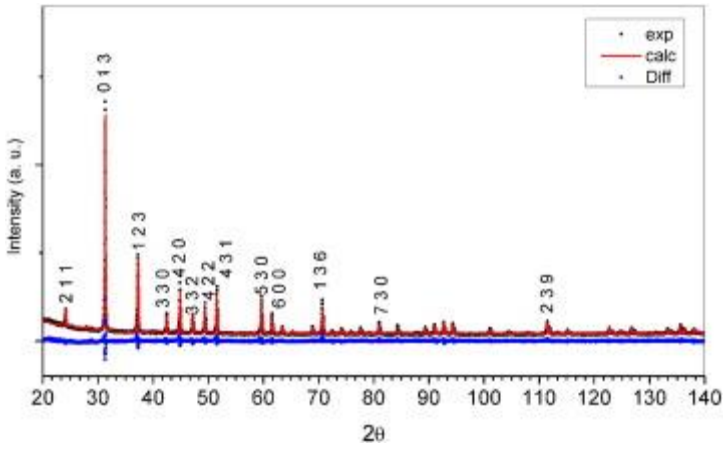
exp
calc
Diff
Intensity (a. u.)
211
013
123
330
420
332
422
431
530
600
136
730
239
20
30
40
50
60
70
80
90
100
110
120
130
140
2θ